Submitted to the
International Conference on High Energy Physics
16-22 August 2004, Beijing, China

Abstract: 5-332, 11-333

Session: QCD hard interactions and Heavy quarks

Inclusive charm jet cross sections in photoproduction

ZEUS Collaboration

Abstract

Differential inclusive jet cross sections for events containing D^* have been measured with the ZEUS detector at HERA using an integrated luminosity of 78.6 pb^{-1}. The measurements have been performed in the photoproduction regime $Q^2 < 1$ GeV^2, for photon-proton centre-of-mass energies in the range $130 < W < 280$ GeV. The measurements are compared with next-to-leading-order QCD calculations.

1 Introduction

Heavy quark production can be calculated using perturbative QCD (pQCD), since a hard scale is given by the heavy quark mass. However, next-to-leading-order (NLO) QCD predictions calculated in either the 'massive' or 'massless' charm schemes do not describe well measurements of inclusive D^* photoproduction cross sections [1, 2]. Examples of charm production processes are shown in Fig. 1 where diagrams (a) and (b) are Leading Order (LO) processes in both sets of calculations. In 'massive' calculations, charm quarks are not active partons in the parton density functions (PDFs), hence processes (c) and (d) only appear at NLO whereas in 'massless' calculations they are LO.

This paper presents inclusive jet cross sections for events containing a charm quark and a jet of high transverse energy, $E_T^{\rm jet}$. The additional hard scale should reduce the dependence of the cross section on uncertainties due to hadronisation effects. Those jets that are associated with a D^* meson are compared to NLO calculations using the 'massive' charm scheme. Jets which are not associated to the D^* meson are also compared to the 'massless' charm pQCD predictions.

2 Analysis

The data presented in this analysis were collected with the ZEUS detector at HERA during the 1998-2000 running periods, with a positron/electron beam of energy $E_e = 27.5$ GeV colliding with a proton beam of energy $E_p = 920$ GeV. The data sample corresponds to an integrated luminosity of 78.6 pb^{-1}.

The measurement was restricted to the photoproduction regime $Q^2 < 1$ GeV^2 with the γp centre-of-mass energy, W, between 130 and 280 GeV. The lower W cut was set by the trigger conditions whereas the upper value rejected deep inelastic scattering events in which the scattered positron was misidentified.

The charm quark was tagged by the identification of $D^{*\pm}(2010)$ mesons in the final state via the charged products of the decay using the ΔM method [3]. The decay channel considered is $D^{*\pm} \rightarrow D^0\pi_s^\pm \rightarrow (K^\mp\pi^\pm)\pi_s^\pm$. The cuts on the tracks identified as the decay products of the D^* meson are as detailed in a previous publication [4]. The D^* meson kinematic region is $|\eta(D^*)| < 1.5$ and $p_T(D^*) > 3$ GeV.

In addition to a D^* meson, at least one jet, reconstructed with the k_T cluster algorithm [5] in its longitudinally invariant inclusive mode [6], was also required. To reconstruct the hadronic final state in the data, the k_T clustering algorithm was applied to energy flow objects, which combine tracking and calorimeter information. Jets were required to be in the region $E_T^{\rm jet} > 6$ GeV and $-1.5 < \eta^{\rm jet} < 2.4$.

After all the above requirements, the mass-difference distribution is shown in Fig. 2 where a clean peak over a relatively low background can be seen. The number of D^* mesons found after subtraction of the background was 4861 $\pm$ 113.

Distributions were also measured for jets associated with identified D^* mesons. Those jets without an associated D^* mesons were defined as 'other' jets. Both in the data and in the reconstructed Monte Carlo (MC) events, a jet and a D^* meson were associated with each other by considering the separation in $\eta - \phi$ space, ΔR. The variable ΔR, defined as $\Delta R = \sqrt{(\eta(D^*) - \eta^{\rm jet})^2 + (\phi(D^*) - \phi^{\rm jet})^2}$, was required to be less than 0.6 for the jet closest to the D^* meson. For jets of hadrons, the D^* meson is clustered into a jet by the k_T algorithm and the final state kaon and pions removed and hence the D^* meson is uniquely associated with one jet.

The MC programs Pythia 6.156 [7] and Herwig 6.301 [8,9] were used to determine the data selection efficiencies and acceptance corrections. The generated event samples were passed through the detector simulation and the same offline reconstruction and analysis cuts as were used for the data.

Systematic uncertainties on the measured cross sections were determined by changing the selection criteria. The variation by one sigma of the resolution for a particular variable was determined from the MC. All systematic uncertainties were within the statistical precision of the measurement. The largest uncertainty arose from that due to the jet energy scale which was varied by 3% leading to a variation in the cross section of $5 - 10\%$.

3 Theoretical Predictions

A fixed order 'massive' calculation from Frixione et al. [10, 11] used CTEQ5M1 [12] for the proton PDF and GRV-HO [13] for the photon PDF. The renormalisation scale was defined as $\mu_R = m_T = \sqrt{m_c^2 + p_{c,T}^2}$, where m_c and $p_{c,T}$ are the pole mass and average transverse momentum of the charm quark, respectively. The factorisation scale was also set to $\mu_F = m_T$. The nominal charm quark mass was set to $m_c = 1.5$ GeV. To estimate the upward theoretical uncertainty, the charm mass was varied to $m_c = 1.3$ GeV simultaneously with $\mu_R = \frac{m_T}{2}$. For the lower value, the charm mass was varied to $m_c = 1.7$ GeV simultaneously with $\mu_R = 2m_T$. The quark fragmentation into a D^* was performed using the Peterson function [14].

The pQCD 'massless' scheme [15,16] predictions from G. Heinrich et al. [17] use AFG [18] for the photon PDF; GRV-HO was also considered and the difference were small. For the proton, the MRST [19–21] PDF was used. The difference between MRST01 and MRST03 proton PDF's was found to be negligible for the distributions considered. The total number of flavours considered was five except for AFG where only four flavours were possible.

The D^* fragmentation function comes from a fit to charm jet data from LEP; the function should be applicable at HERA as they are derived using the factorisation theorem in QCD. The central prediction uses a renormalisation scale $\mu_R = m_T = \sqrt{m_c^2 + p_T(D^*)^2}$, where $m_c = 1.5$ GeV and $p_T(D^*)$ is the transverse momentum of the D^* meson. The factorisation, μ_F, and fragmentation, M, scales are set to $M = \mu_F = 2m_T$. The uncertainty comes from changing the scales to $\mu_R = \frac{m_T}{2}$ and $\mu_F = 4m_T$ for the upper bound, and $\mu_R = 2m_T$ and $\mu_f = m_T$ for the lower bound.

As the NLO calculations contain partons in the final state, the effects of hadronisation are considered when comparing the predictions with the data. The NLO QCD predictions were corrected for hadronisation effects using a bin-by-bin procedure according to $d\sigma = d\sigma^{\rm NLO} \cdot C_{\rm had}$, where $d\sigma^{\rm NLO}$ is the cross section for partons in the final state of the NLO calculation. The hadronisation correction factor was defined as the ratio of the jet cross sections before and after the hadronisation process, $C_{\rm had} = d\sigma^{\rm hadrons}_{\rm MC}/d\sigma^{\rm partons}_{\rm MC}$. The value of $C_{\rm had}$ was taken as the mean of the ratios obtained using the HERWIG and PYTHIA predictions. The uncertainty due to the hadronisation correction was estimated as half the spread between the values obtained using the two MC models.

4 Inclusive Jet Cross Sections Results

Inclusive jet cross sections with a D^* in the final state have been measured as a function of $E_T^{\rm jet}$ and $\eta^{\rm jet}$ in the following kinematic region: $Q^2 < 1$ GeV^2, $130 < W < 280$ GeV, $p_T(D^*) > 3$ GeV, $|\eta(D^*)| < 1.5$, $E_T^{\rm jet} > 6$ GeV and $-1.5 < \eta^{\rm jet} < 2.4$. In Fig. 3, cross-sections $d\sigma/dE_T^{\rm jet}$ in bins of $\eta^{\rm jet}$ are shown, for the whole $\eta^{\rm jet}$ region and differentially in four bins of $\eta^{\rm jet}$. Figure 4 shows cross-sections $d\sigma/d\eta^{\rm jet}$ in bins of $E_T^{\rm jet}$, for the whole range of $E_T^{\rm jet}$ and for low and high $E_T^{\rm jet}$. Cross sections measured separately for D^* jets and other jets are shown in Fig. 5 for $d\sigma/dE_T^{\rm jet}$ and in Fig. 6 for $d\sigma/d\eta^{\rm jet}$.

The 'massive' QCD predictions generally reproduce the shape of all distributions for all jets, D^* jets and 'other' jets. However, the central pQCD predictions underestimate the data over the whole range in $E_T^{\rm jet}$ and $\eta^{\rm jet}$. For even the most extreme changes in scale and mass, the predictions are somewhat below the data. The largest differences are seen at higher $E_T^{\rm jet}$ compared to the 'massive' QCD predictions.

The 'massless' calculations can only be compared to the 'other' jet distributions. Figure 5, $d\sigma/dE_T^{\rm jet}$, shows that the 'massless' pQCD prediction has theoretical uncertainties of the same order as the 'massive' scheme and better agreement at high $E_T^{\rm jet}$. However, the general features are the same as for the 'massive' prediction; the shape is reasonably well described and the upper theoretical prediction agrees with the normalisation of the data. The resolved contribution is also shown which decreases at high $E_T^{\rm jet}$. For $d\sigma/d\eta^{\rm jet}$, shown in Fig. 6, the shape of the data are also well described by the 'massless' calculation. The resolved contribution is up to $80-90\%$ in the forward $\eta^{\rm jet}$ region.

5 Summary

Charm jet production has been measured in photoproduction and compared to available NLO QCD predictions in both the 'massive' and 'massless' schemes. At high jet transverse energy, where the 'massless' scheme is expected to be more reliable, predictions from the 'massless' calculation are somewhat above those from the 'massive' scheme and are closer to the data. In order for both types of calculation to achieve a reasonable description of the shape of the data, particularly as a function of $\eta^{\rm jet}$, effects of hadronisation, modelled using Monte Carlo programs, have to be taken into account. The overall normalisation of the theoretical predictions is below that of the data but agrees within the large uncertainties arising from the theory.

Acknowledgements

We thank G. Heinrich for useful discussions.

References

[1] ZEUS Coll., *Measurement of $D^{*\pm}$ photoproduction at HERA* (unpublished). Submitted to the 31th International Conference on High-Energy Physics, ICHEP2002, Amsterdam, The Netherlands, July 2002.

[2] H1 Coll., *Photoproduction of $D^{*\pm}$ at HERA* (unpublished). Submitted to the International Europhysics Conference on High Energy Physics, EPS03, Aachen, Germany, July 2003.

[3] S. Nussinov, Phys. Rev. Lett. **34**, 1286 (1975).

[4] ZEUS Coll., S. Chekanov et al., Phys. Lett. **B 565**, 87 (2003).

[5] S.Catani et al., Nucl. Phys. **B 406**, 187 (1993).

[6] S.D. Ellis and D.E. Soper, Phys. Rev. **D 48**, 3160 (1993).

[7] T. Sjöstrand et al., Comp. Phys. Comm. **135**, 238 (2001).

[8] G. Marchesini et al., Preprint Cavendish-HEP-99/17 (hep-ph/9912396), 1999.

[9] G. Corcella et al., Preprint hep-ph/0107071, 2001.

[10] S. Frixione et al., Adv. Ser. Direct. High Energy Phys. **15**, 609 (1998).

[11] S. Frixione et al., Nucl. Phys. **B 412**, 225 (1994).

[12] CTEQ Coll., H.L. Lai et al., Eur. Phys. J. **C 12**, 375 (2000).

[13] M. Glück, E. Reya and A. Vogt, Z. Phys. **C 53**, 127 (1992).

[14] C. Peterson et al., Phys. Rev. **D 27**, 105 (1983).

[15] M. Fontannaz, J.P. Guillet and G. Heinrich, Eur. Phys. J. **C 26**, 209 (2002).

[16] M. Fontannaz, J.P. Guillet and G. Heinrich, Eur. Phys. J. **C 21**, 303 (2001).

[17] G. Heinrich, private communication, 2004.

[18] P. Aurenche, J.P. Guillet and M. Fontannaz, Z. Phys. **C 64**, 621 (1994).

[19] A.D. Martin et al., Nucl. Phys. Proc. Suppl. **B 79**, 105 (1999). *Proc. 7^{th} Int. Workshop on Deep Inelastic Scattering and QCD (DIS99),* J. Blümlein and T. Riemann (eds.). Zeuthen, Germany, April 1999.

[20] R.S. Thorne et al., Preprint hep-ph/0106075, 2001.

[21] A.D. Martin et al., Preprint hep-ph/0110215, 2001.

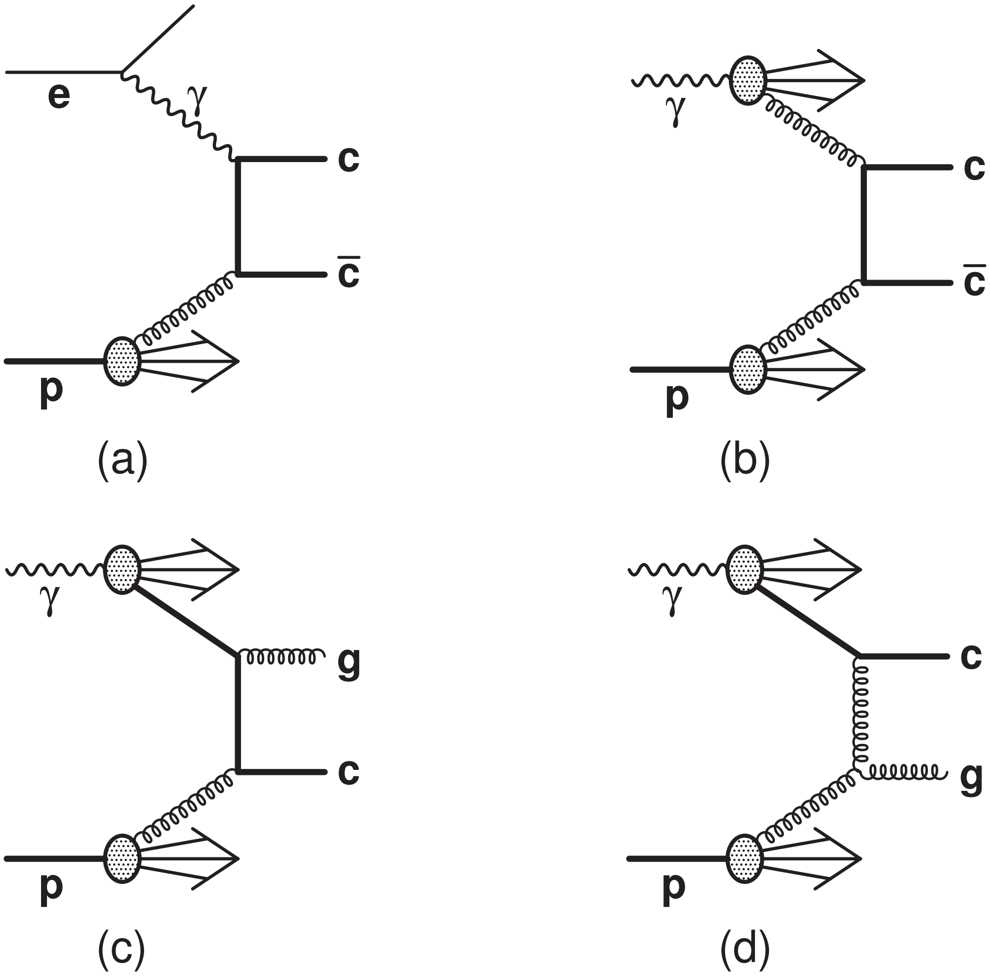

Figure 1: *Leading order QCD charm-production diagrams. a) direct photon: $\gamma g \to c\bar{c}$; b) resolved photon: $gg \to c\bar{c}$; c) resolved-photon charm excitation: $cg \to gc$ (c in proton hemisphere); d) resolved-photon charm excitation: $cg \to cg$ (c in the photon hemisphere).*

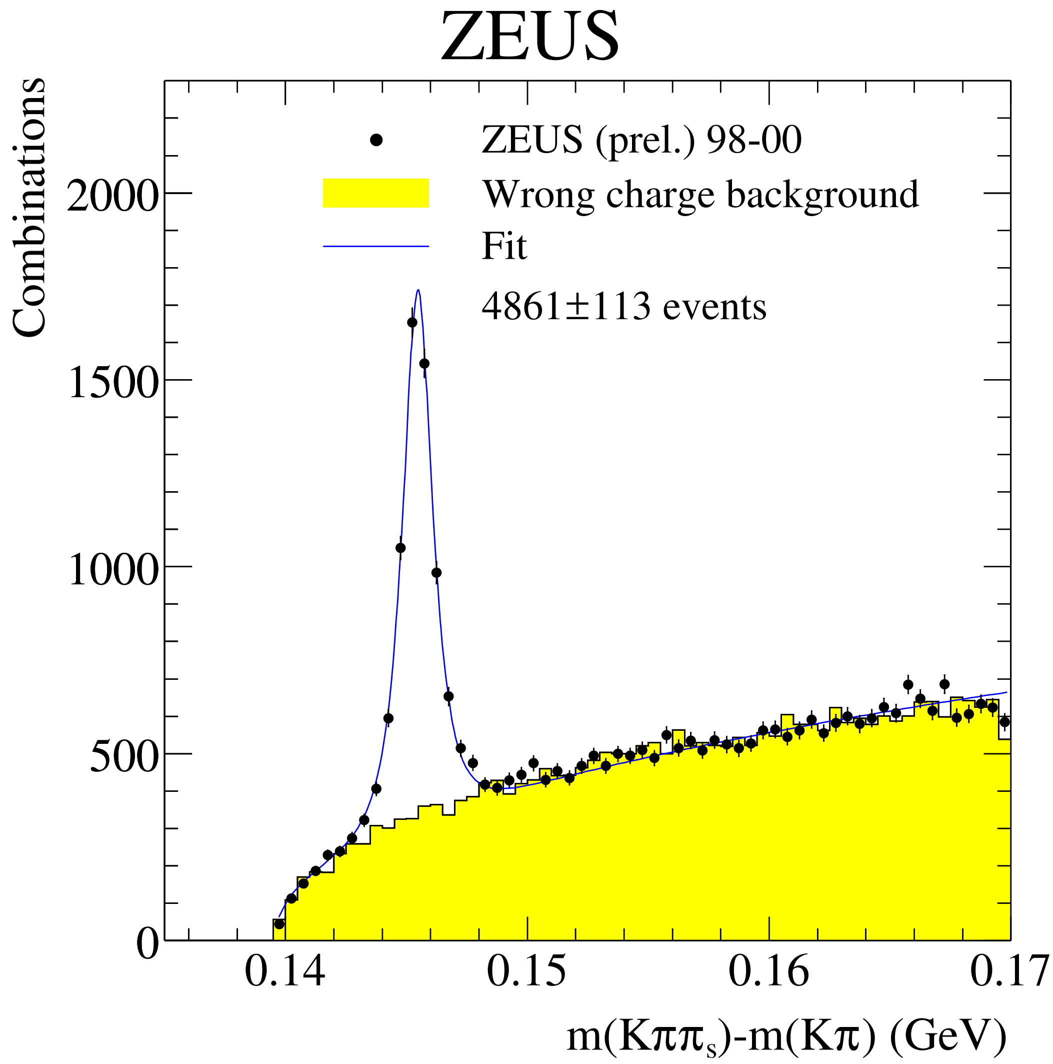

Figure 2: *The distribution of the mass difference, $\Delta M = M(K\pi\pi_s) - M(K\pi)$, for $D^{*\pm}$ candidates (solid dots). The histogram shows the ΔM distribution for wrong charge combinations. Only $D^{*\pm}$ candidates from the region $0.143 < \Delta M < 0.148$ GeV were used for the cross-section measurement.*

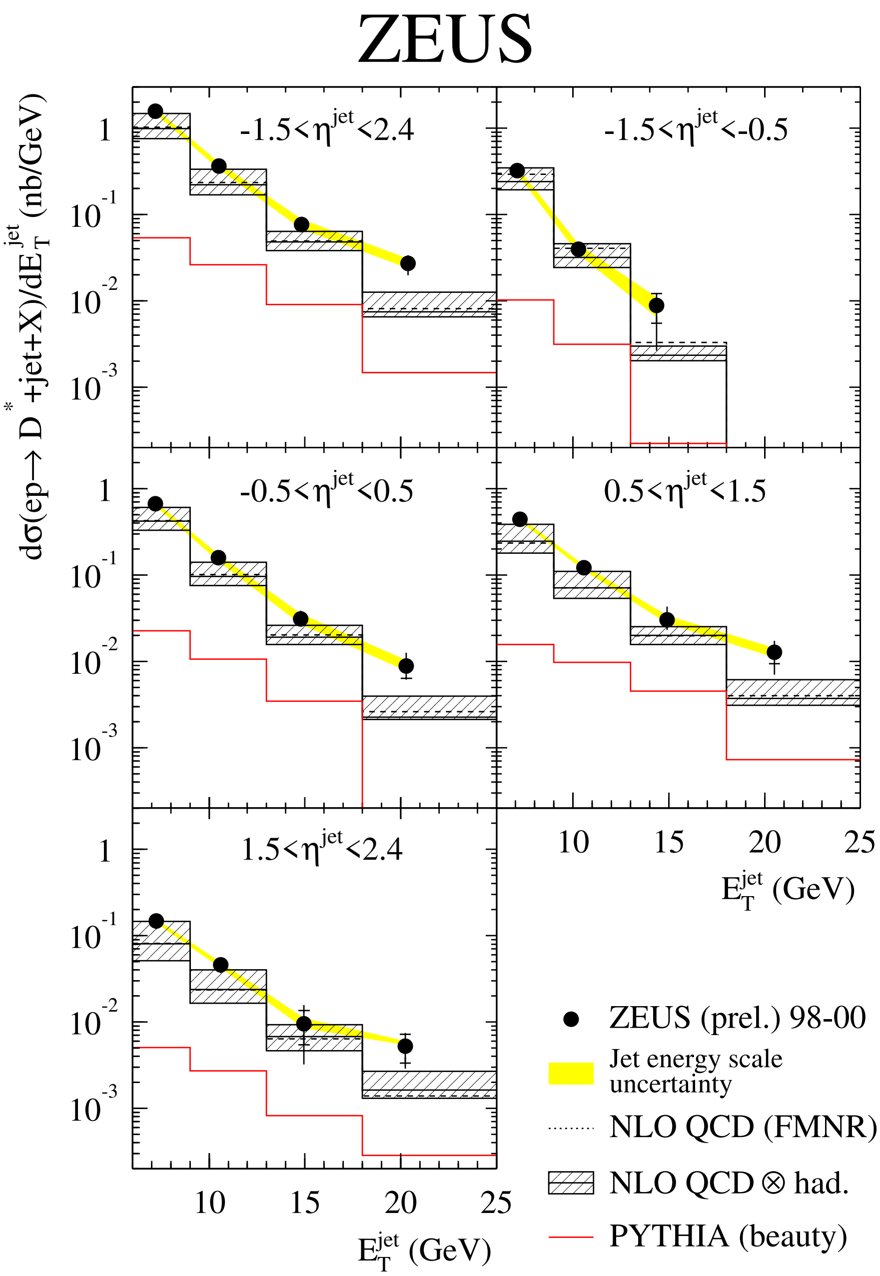

Figure 3: *Cross-section $d\sigma/dE_T^{\mathrm{jet}}$ for jets in events (dots) containing at least one $D^{*\pm}$ meson for the whole η^{jet} range possible and double differentially going from backwards to forwards in η^{jet}. The comparison is made to 'massive' pQCD predictions with (solid line) and without (dotted line) hadronisation corrections applied. The theoretical uncertainties (hatched band) come from the change in renormalisation scale simultaneously with the change in charm mass. The beauty component is also shown (lower histogram) as given from PYTHIA.*

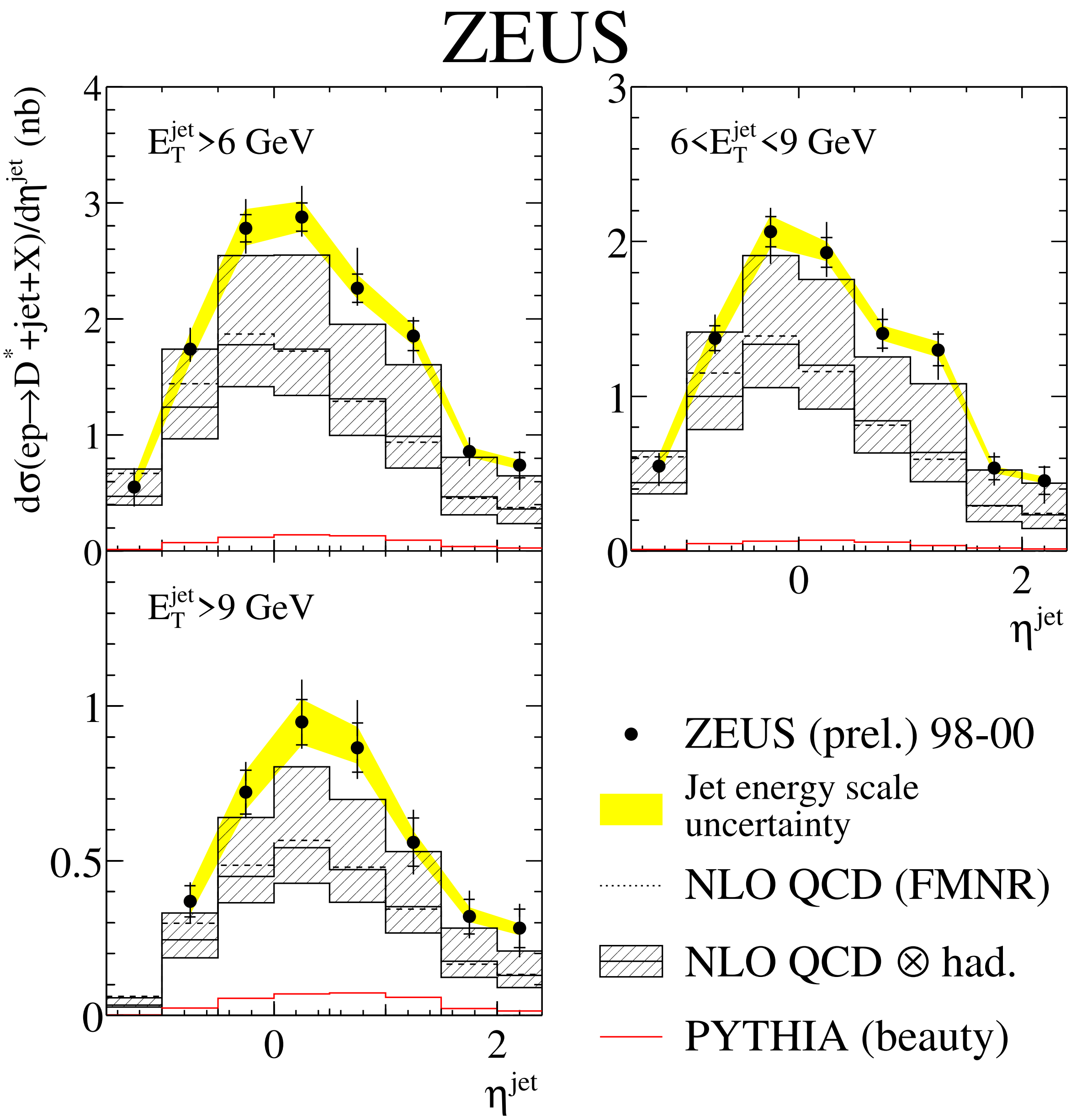

Figure 4: *Cross-section $d\sigma/d\eta^{\rm jet}$ for jets in events (dots) containing at least one $D^{*\pm}$ meson for the whole $E_T^{\rm jet}$ range possible and double differentially for low and high $E_T^{\rm jet}$. The comparison is made to 'massive' pQCD predictions with (solid line) and without (dotted line) hadronisation corrections applied. The theoretical uncertainties (hatched band) come from the change in renormalisation scale simultaneously with the change in charm mass. The beauty component is also shown (lower histogram) as given from PYTHIA.*

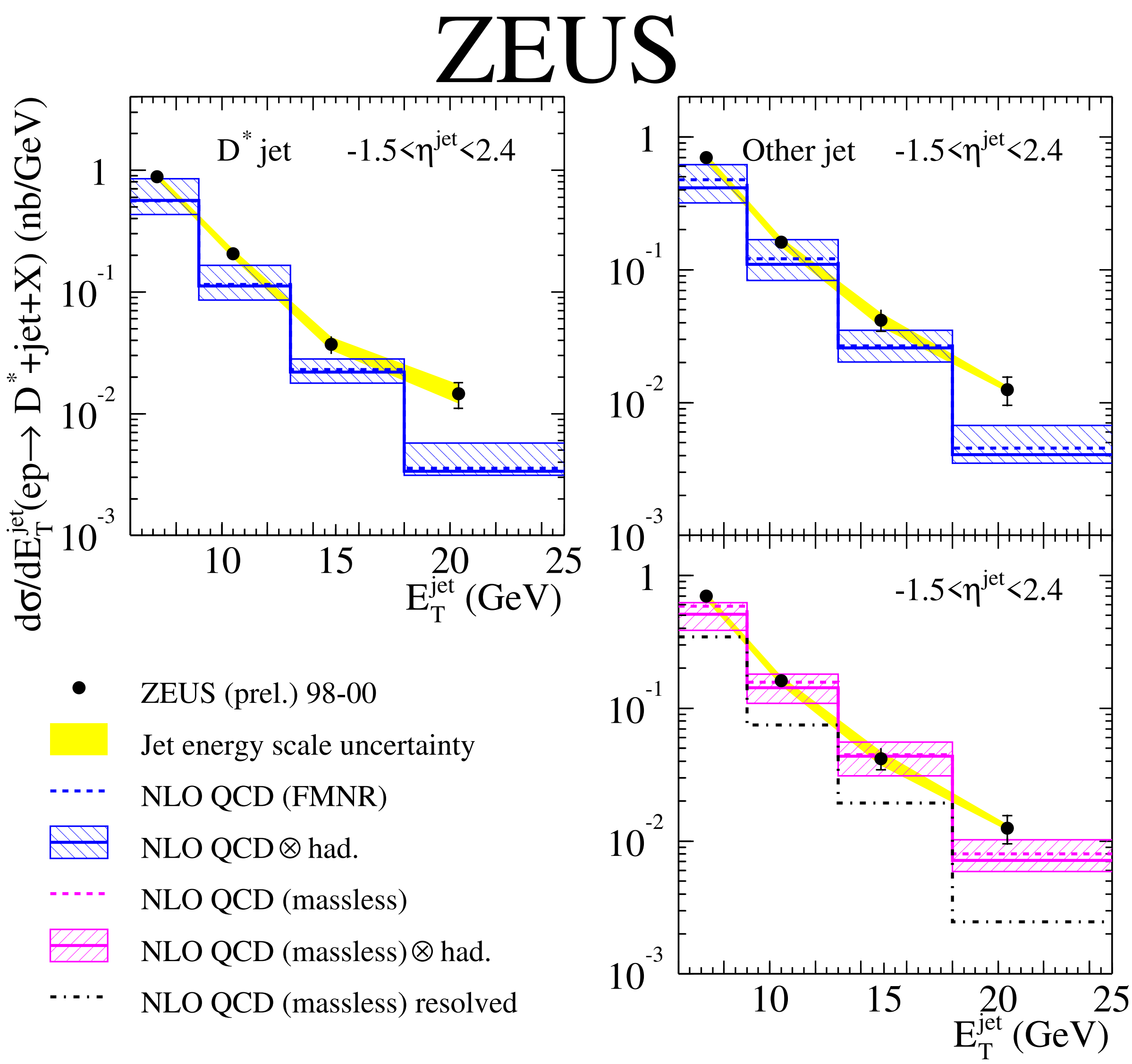

Figure 5: *Cross-section $d\sigma/dE_T^{\rm jet}$ for D^* jets and other jets (dots). The comparison is made to 'massive' pQCD predictions with (solid line) and without (dotted line) hadronisation corrections applied. The theoretical uncertainties (hatched band) come from the change in renormalisation scale simultaneously with the change in charm mass, as detailed in the text. For the other jet distribution, the 'massless' pQCD predictions are shown with (solid line) and without (dotted line) hadronisation corrections applied. The uncertainties (hatched band) come from the change in initial and final factorisation parameterisation. The resolved contributions for the 'massless' calculation are shown (dashed line).*

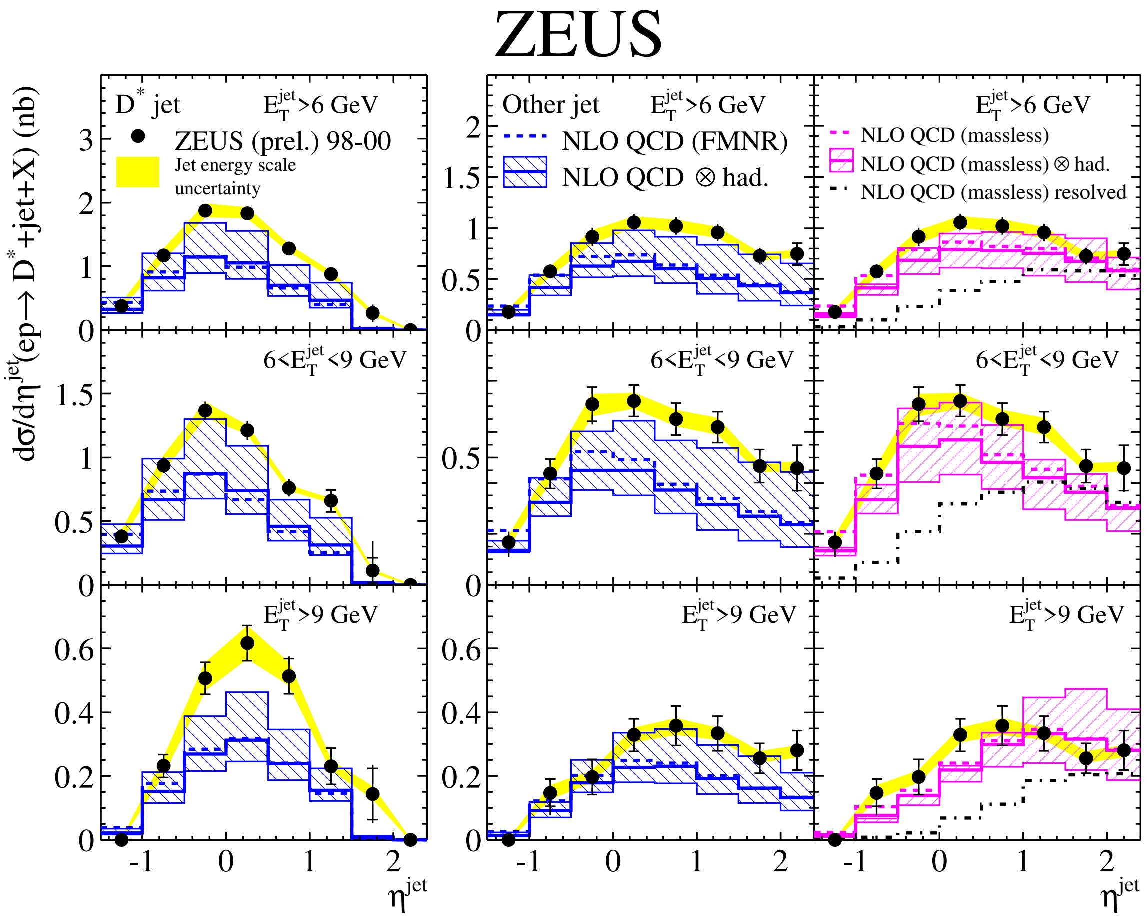

Figure 6: *Cross-section $d\sigma/dE_T^{\rm jet}$ for D^* jets and other jets (dots) for the whole $E_T^{\rm jet}$ range possible and double differentially for low and high $E_T^{\rm jet}$. The comparison is made to 'massive' pQCD predictions with (solid line) and without (dotted line) hadronisation corrections applied. The theoretical uncertainties (hatched band) come from the change in renormalisation scale simultaneously with the change in charm mass, as detailed in the text. For the other jet distribution, the 'massless' pQCD predictions are shown with (solid line) and without (dotted line) hadronisation corrections applied. The uncertainties (hatched band) come from the change in initial and final factorisation parameterisation. The resolved contributions for the 'massless' calculation are shown (dashed line).*